



One-dimensionality of thermoelectric properties of semiconducting nanomaterials

Yota Ichinose,¹ Manaho Matsubara ,² Yohei Yomogida,¹ Akari Yoshida,¹ Kan Ueji ,¹ Kaito Kanahashi,³ Jiang Pu,⁴ Taishi Takenobu,⁴ Takahiro Yamamoto,² and Kazuhiro Yanagi¹

¹*Department of Physics, Tokyo Metropolitan University, Tokyo 192-0397, Japan*

²*Department of Physics, Tokyo University of Science, Shinjuku, Tokyo 162-8601, Japan*

³*Department of Advanced Science and Engineering, Waseda University, Tokyo 169-855, Japan*

⁴*Department of Applied Physics, Nagoya University, Aichi 464-8603, Japan*



(Received 13 June 2020; accepted 12 February 2021; published 26 February 2021)

Thermoelectric conversion, which is the generation of electricity from waste heat, can play an important role in renewable energy use. Lowering the dimensionality of semiconductor thermoelectric materials is a promising approach for improving thermoelectric performance, and ultimately one-dimensional (1D) semiconductor materials have the potential to exhibit maximized performance because of the presence of a 1D electronic structure, such as the van Hove singularity (vHs) in the density of states. However, experimentally verifying the effect of the 1D nature on the thermoelectric performance in semiconductor nanomaterials has been difficult because we cannot observe any traces of the 1D electronic structure in terms of conventional thermoelectric parameters, such as the Seebeck coefficient or power factor. Here, we show that a thermoelectric parameter, the thermoelectrical conductivity (L_{12}), is strongly correlated with the electronic structure and exhibits a unique 1D trace with single-walled carbon nanotubes (SWCNTs). We experimentally clarify that the L_{12} of high-purity semiconducting SWCNTs has a peak structure with a chemical potential in the vicinity of the vHs. For comparison, the L_{12} of monolayer molybdenum disulfides and graphene, which are chosen as 2D models, shows a different behavior, simply exhibiting constant values. Furthermore, we find that theoretical calculations support these L_{12} behaviors, which are consistent with the expected behaviors of 1D and 2D electronic structures. Our results demonstrate that L_{12} is a very good parameter for evaluating the traces of dimensionalities, thereby advancing the elucidation of the fundamental thermoelectric properties necessary for the development of low-dimensional materials.

DOI: [10.1103/PhysRevMaterials.5.025404](https://doi.org/10.1103/PhysRevMaterials.5.025404)

I. INTRODUCTION

The demand for flexible high-performance thermoelectric materials to power wearable electronics and sensors has been increasing [1]. Semiconductor materials with low dimensions have been pursued for their superior thermoelectrics, as predicted in seminal papers by Hicks and Dresselhaus [2]. In particular, one-dimensional (1D) semiconductor materials are expected to achieve the highest performance due to the decrease in thermal conductivity and the formation of 1D electronic structures, such as the van Hove singularity (vHs) in the density of states (DOS) [3,4]. The former factor has been experimentally confirmed by many studies [5,6]; however, the experimental verification of how the 1D electronic structure influences the thermoelectric properties remains elusive. One of the reasons is that it is very difficult to discuss the dimensionalities of conventional thermoelectric parameters, such as the Seebeck coefficient S and power factor P . For example, within conventional theoretical models, such as the Boltzmann transport theory with a constant relaxation-time approximation and an effective-mass approximation, S within the band gap of a d -dimensional ($d = 1, 2, 3$) semiconductor as a function of the chemical potential μ can be expressed as

$$S = \frac{k_B}{q} \left(\frac{d}{2} - \frac{\mu}{k_B T} + 1 \right), \quad (1)$$

where k_B is Boltzmann's constant, q is the charge of carriers, and T is the temperature [7]. Equation (1) indicates that the difference in d does not influence the line shapes of S as a function of μ . Thus, the doping dependence of S , i.e., the shift of μ , never signals the dimensionality. These characteristics make it difficult to understand how lowering the dimensions of materials enhances the thermoelectric performance, except for the apparent tendency of lowering the thermal conductivity.

However, recently a theoretical study using the linear-response theory by Yamamoto and Fukuyama noted the importance of the L_{12} term, which they called the "thermoelectrical conductivity," for understanding the thermoelectric properties of nanomaterials [8]. Here, we briefly discuss their notations. The current density J in the presence of an electric field E and a temperature gradient dT/dx along the x -direction is described as

$$J = L_{11}E - \frac{L_{12}}{T} \frac{dT}{dx} \quad (2)$$

when there is a temperature difference ΔT and an induced voltage ΔV between the two ends of the materials, where $E = -\Delta V/L$ and $dT/dx = \Delta T/L$ for a spatially uniform system

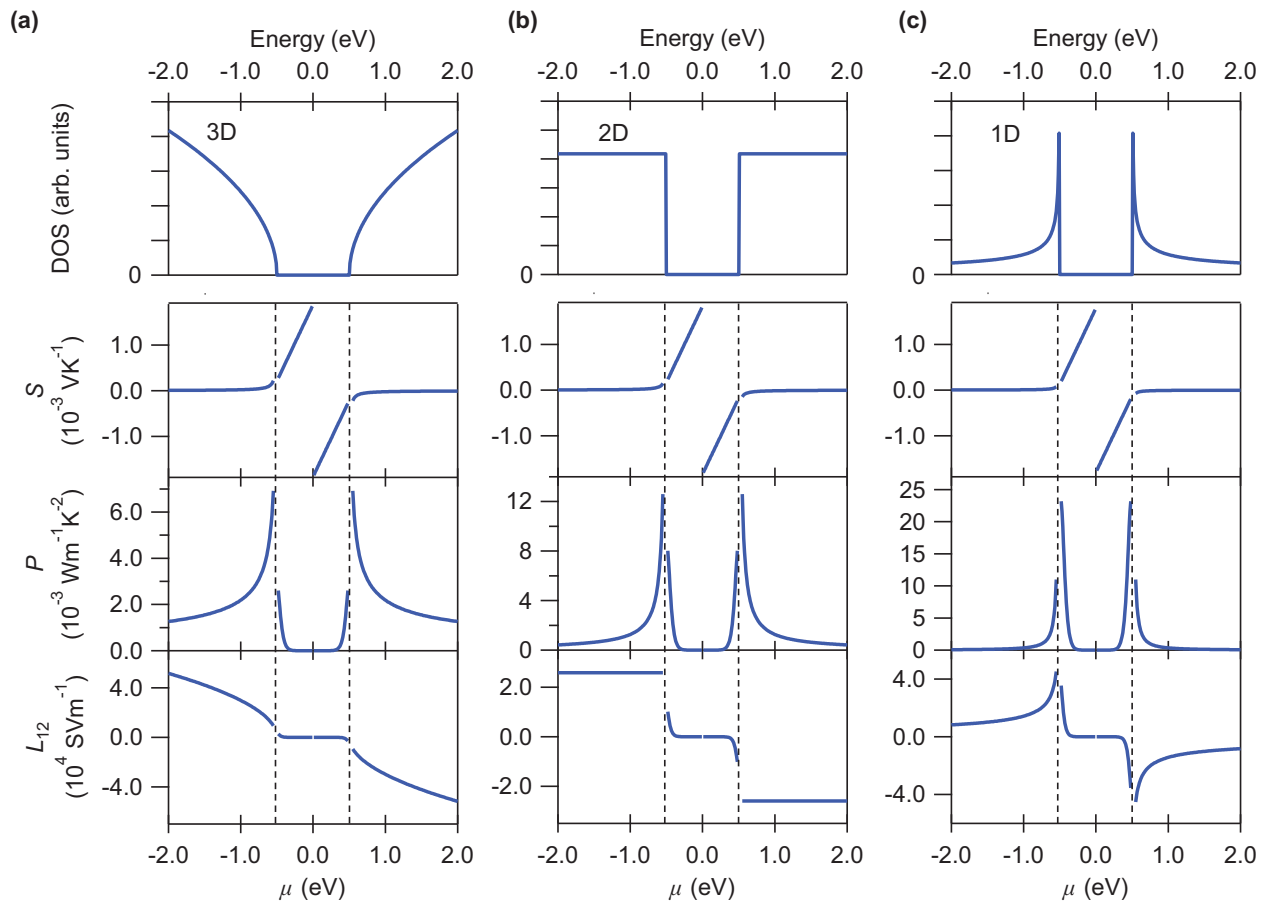


FIG. 1. Thermoelectric properties for homogeneous semiconductors calculated using the Boltzmann transport theory within an effective-mass approximation. The top panels show the energy dependence of the density of states (DOS) for (a) 3D, (b) 2D, and (c) 1D structures. Underneath the top row and from top to bottom, the panels show the Seebeck coefficient (S), power factor (P), and thermoelectrical conductivity (L_{12}) as a function of chemical potential (μ) for an effective mass $m^* = 9.11 \times 10^{-31}$ kg, a relaxation time $\tau = 100$ fs, and a unit-cell length $a = 1$ nm at $T = 300$ K. The vertical axes of (b) and (c) are the same as those in (a). The band edges of the valence and conduction bands for all semiconductors are set to ± 0.5 eV (dotted lines). Details are provided in Table S1 of the SM.

with length L . L_{11} corresponds to the electrical conductivity σ . According to the definition, S is expressed as $S = L_{12}/T\sigma$. Yamamoto and Fukuyama's paper implied that the structure of the DOS significantly affected the line shape of the L_{12} term. The line shape of the DOS reflects the dimensionality of the electronic structure of the samples, suggesting that traces of the dimensionalities can be found in the L_{12} term. The clarification of the independent thermoelectric parameter, which strongly couples with the dimensionality of the electronic structure or the structure of the DOS, will provide a bottom-up strategy for applying low-dimensional effects to improve thermoelectric performance.

Therefore, in this study, first we theoretically discuss the relationships between the dimensionality and thermoelectric parameters, including L_{12} , in the Boltzmann transport theory framework, and then we discuss the line shapes of L_{12} using actual samples that utilize semiconducting single-walled carbon nanotubes (SWCNTs), which are 1D models. We compare these line shapes with the L_{12} line shape of molybdenum disulfide (MoS_2) and graphene, which are 2D models, and then we demonstrate how the 1D characteristics appear in the L_{12} of semiconducting SWCNTs.

II. RESULTS AND DISCUSSION

A. Relationships between dimensionality and thermoelectric properties

First, we briefly discuss the relationships among the dimensionalities, S , P , and L_{12} . Figure 1 describes the calculated DOS, S , P , and L_{12} for semiconductor models with 1D, 2D, and 3D electronic structures. Here, we plot the figures by setting the potential of μ at the charge neutral point as zero. The calculations are performed within the Boltzmann transport theory with a constant relaxation-time approximation and effective-mass approximation. Note that the Boltzmann transport theory cannot apply to the disordered state in the energy region around the band edges. The detailed calculation method is provided in the supplemental material (SM) [9]. As shown in the figures, although the line shapes of the DOS change depending on the dimensionalities, the line shapes of S are similar among all the dimensions. Regarding P , the value just becomes the maximum around the band edge in any dimensionality, and the line shapes are almost the same. Therefore, we cannot distinguish the dimensionalities of the samples from the conventional thermoelectric parameters S

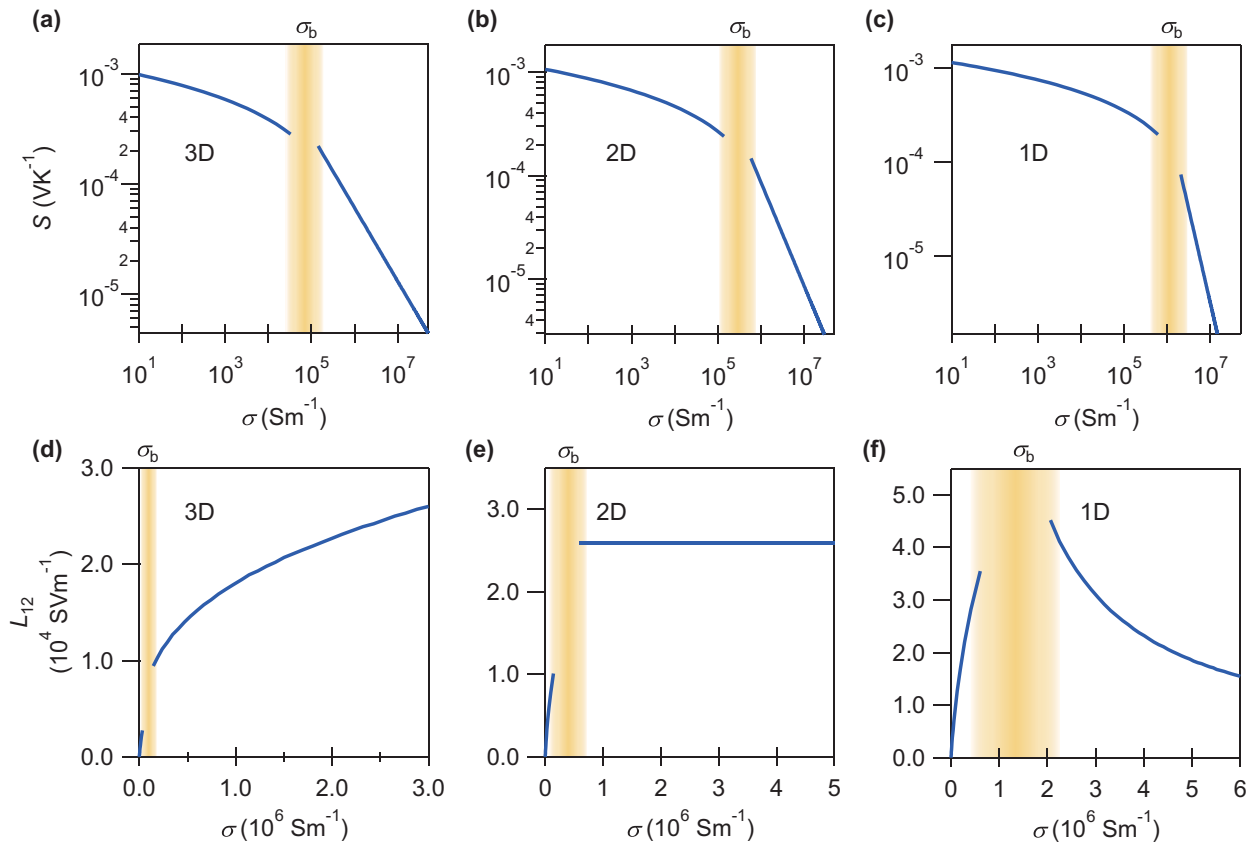


FIG. 2. Thermoelectric parameters as a function of electrical conductivity (σ), calculated using the Boltzmann transport theory within an effective-mass approximation. The relationship is shown between the Seebeck coefficient (S) and σ for the (a) 3D, (b) 2D, and (c) 1D structures. σ at the band edge is described as σ_b (yellow gradient color). The vertical axes of (b) and (c) are the same as those in (a). The relationship is shown between thermoelectrical conductivity (L_{12}) and σ for the (d) 3D, (e) 2D, and (f) 1D structures. The vertical axes of (e) and (f) are the same as those in (d).

and P . However, in the case of L_{12} , the line shapes exhibit distinct characteristics depending on the dimensionalities. The L_{12} values are negligible in all dimensions when μ is located within the band gap. In 3D, the absolute values of L_{12} increase monotonically as μ shifts from the band-edge position. However, in 2D, the values are constant, and in 1D, the value becomes the maximum around the band edge and decreases as μ shifts from the band edge. These simple theoretical analyses clearly indicate that L_{12} is a good parameter to discuss the dimensionalities of thermoelectric properties.

From an experimental point of view, it is rather difficult to precisely discuss the thermoelectric parameters as a function of μ . Thus, we plotted the relationship between the thermoelectric parameters and σ in the 3D, 2D, and 1D semiconductors in Fig. 2.

Here, σ at the band edge is described as σ_b . Figures 2(a)–2(c) indicate the relationships between S and σ in the case of the 3D, 2D, and 1D electronic structures. As shown in the figures, it is very difficult to distinguish the dimensionalities from these plots. Figures 2(d)–2(f) indicate the relationships between L_{12} and σ . These panels clearly present the characteristic behaviors that depend on the dimensionalities. In all dimensionalities, when μ is located within the band gap, i.e., $\sigma < \sigma_b$, L_{12} increases as σ increases. When μ is located outside the band gaps, i.e., $\sigma > \sigma_b$, in the 3D case

L_{12} increases as σ increases, and in the 2D case L_{12} stays constant, whereas in the 1D case L_{12} decreases as σ increases. Therefore, L_{12} strongly reflects the dimensionalities of the electronic structure of materials, indicating that we can deduce the dimensionality of samples from this term. Thus, to clarify this point, we experimentally investigated the L_{12} term with SWCNTs.

B. Effect of the dimensionality of semiconducting SWCNTs on the thermoelectric properties

SWCNTs are one of the most suitable materials for tackling this subject because they have a sharp vHs in the DOS of their individual states. Since the discovery of SWCNTs, many studies have been conducted regarding the thermoelectric properties of SWCNTs in their individual and thin-film forms (see a recent review) [10]. Regarding the topic of the 1D characteristics of thermoelectric properties, a recent paper revealed the uniqueness of the 1D thermoelectric properties of the “metallic” type as breaking the thermoelectric tradeoff [11], but not the “semiconducting” type, because, as discussed above, we cannot identify the 1D characteristics in the behavior of conventional thermoelectric parameters in the case of semiconductors. Here, we focused on the thermoelectrical conductivity, namely the L_{12} term, of semiconducting

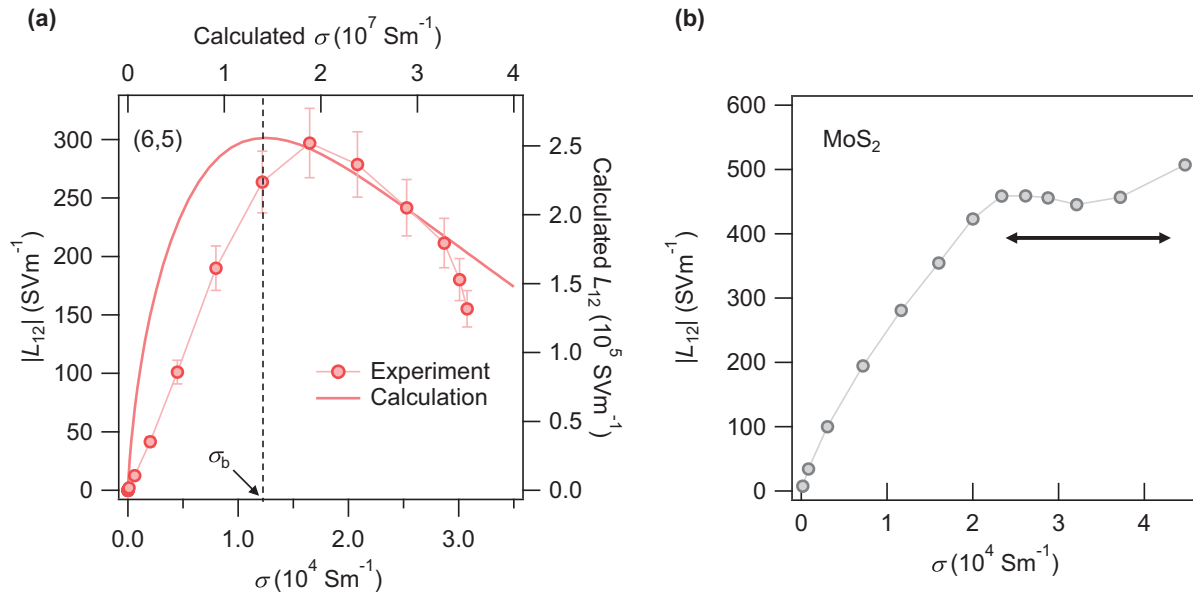


FIG. 3. Experimental results of the thermoelectrical conductivity (L_{12}) as a function of electrical conductivity (σ). (a) $|L_{12}|$ for (6,5) SWCNTs. σ at the band edge is described as σ_b , which is obtained by analyzing the relationship between the power factor and σ (see Fig. S3 of the SM). A solid line presents the result of the theoretical calculation by the Kubo-Luttinger theory. Details about the calculations are provided in Sec. IV of this paper and in Fig. S4 of the SM. The relative error in L_{12} is $\sim 10\%$, calculated from the Seebeck coefficient measurement errors of the devices. (b) $|L_{12}|$ for monolayer MoS_2 as a representative 2D semiconducting material. The data are reanalyzed from Ref. [15] for MoS_2 . The result as a function of gate voltage is shown in Fig. S5 of the SM.

SWCNTs to verify the traces of the vHs on the thermoelectric properties.

To experimentally investigate the thermoelectric properties over a wide range of carrier densities, we systematically controlled the carrier injection by an electrolyte gating technique, which is a method used in previous studies [11,12]. We depict a schematic image of the measured device in Fig. S1 of the SM. By changing the gate voltage V_G , the carrier injection is precisely controlled. L_{12} and P are obtained experimentally by measuring σ and S at each V_G . On the other hand, it is rather difficult to precisely determine the relationships between the V_G and the location of μ in the SWCNT networks; thus, the L_{12} obtained in this study is plotted and discussed as a function of σ . Details of the experimental setup are written in Sec. IV. To systematically understand the relationships between the electronic structures of semiconducting SWCNTs and the thermoelectric properties, we prepared several kinds of semiconducting SWCNTs, namely (6,5), (9,4), and (10,3) SWCNTs, by gel chromatography [13], and semiconducting SWCNTs with a diameter of 1.4 nm (Semi) by density gradient ultracentrifugation [14].

Figure 3(a) presents the experimental result of the relationship between L_{12} and σ of the (6,5) SWCNTs. Here, to focus on the appearance of the dimensionalities on the data, we plotted only the p -type regions of L_{12} . The full line shapes of L_{12} and the experimental data of S and σ as a function of V_G are described in Fig. S2 of the SM. As shown in the figure, L_{12} exhibits a clear peak structure around $\sigma \sim 1.6 \times 10^4 \text{Sm}^{-1}$ and then gradually decreases as σ increases. The position of σ_b is determined from the power factor versus σ (Fig. S3 of the SM). We find that σ at this peak position almost corresponds to σ_b . Therefore, we find that L_{12} reaches its maximum

around the band edge and decreases as σ increases. These behaviors are similar to the 1D behavior of L_{12} predicted in Fig. 2(f) except for the energy region around the band edges. To evaluate the correctness of the observed behavior of L_{12} , we compare this experimental result to the theoretical calculation based on the Kubo-Luttinger theory, which can apply even to disordered states around band edges [8,16,17]. Here, we used the linear-response theory combined with the thermal Green's function method (see Sec. IV). The calculation results are plotted as a solid line in Fig. 3(a). As shown here, the theoretical calculation based on the 1D Dirac model of (6,5) SWCNTs can reproduce the experimental L_{12} behavior of (6,5) SWCNTs.

For comparison, we checked the L_{12} line shape of monolayer MoS_2 , which is a model for 2D semiconductors. L_{12} is derived from the data of S and σ in Ref. [15]. As shown in Fig. 3(b), in the case of MoS_2 , L_{12} does not show a peak structure but rather a plateau, reflecting the L_{12} behavior of the 2D-like semiconductor [see Fig. 2(e)]. Additionally, we also checked the L_{12} line shape of graphene using the data of S and σ in Ref. [18]. We observe that L_{12} becomes almost constant in the high-conductivity region (see Fig. S5 of the SM). These results indicate that the peak structure of L_{12} can only be observed in (6,5) SWCNTs. Therefore, we conclude that the experimentally observed peak structure of L_{12} in (6,5) SWCNT thin films reflects the 1D trace of the (6,5) SWCNT samples.

Although we find such 1D character in the L_{12} of (6,5) SWCNTs, we sometimes find other-dimensional behavior in other samples. Figure 4 indicates L_{12} versus σ plots in (9,4), (10,3), and Semi SWCNTs. In contrast to the case of (6,5) SWCNTs, we cannot observe clear peak structures in the L_{12}

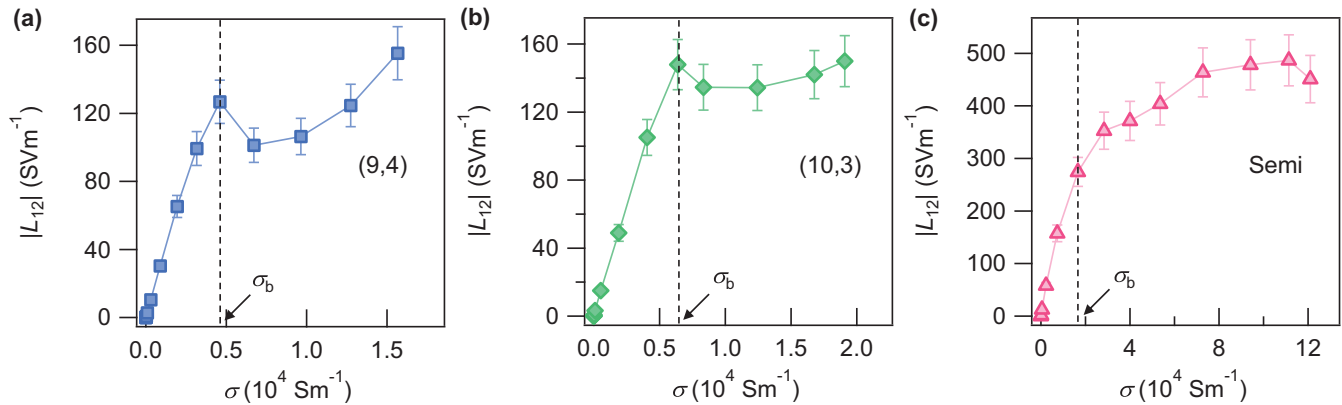


FIG. 4. Chirality dependence of the thermoelectrical conductivity (L_{12}). Experimental results of $|L_{12}|$ in the p -type regions for (a) (9,4), (b) (10,3), and (c) Semi SWCNTs as a function of electrical conductivity (σ). σ at the band edge is described as σ_b , which is obtained by analyzing the relationship between the power factor and σ . The relative error in L_{12} is $\sim 10\%$, calculated from the Seebeck coefficient measurement errors of the devices.

results of (9,4), (10,3), and Semi SWCNTs. In the figures, the position of σ_b is determined from P versus σ (Fig. S3 of the SM). In all of the samples, when $\sigma < \sigma_b$, we observe increases in L_{12} as σ increases. However, the (9,4), (10,3), and Semi SWCNTs did not show a clear decrease in L_{12} as σ increases, when $\sigma > \sigma_b$. In these samples, the L_{12} value becomes constant or increases as σ increases, when $\sigma > \sigma_b$. These behaviors are relatively similar to the L_{12} behaviors in 2D or 3D electronic structures.

To understand the background, we discuss the following two possible mechanisms: (i) the influence of bundle and network formation in films, and (ii) the influence of metallic SWCNTs as impurities. Regarding the former mechanism, in thin films of SWCNTs, the SWCNTs form a bundled structure in which individual SWCNTs are tightly packed and form networks. The bundle formation will broaden the peak of the vHs and will blur the 1D characteristics. SWCNTs with large diameters tend to form bundles more easily than SWCNTs with small diameters [19]. Therefore, we assume that the peak behavior in the L_{12} of large-diameter semiconducting SWCNTs may be blunted by the broadening of the vHs through the formation of strongly bundled structures. In addition, the presence of junctions between the bundles will also contribute to the thermoelectric properties, and these junctions will make the transport in SWCNT networks deviate from that of 1D-like transport. These factors will cause 2D- or 3D-like thermoelectric properties in the thin films of (9,4), (10,3), and Semi SWCNTs.

For the latter mechanism, we describe how the presence of metallic SWCNTs in the sample influences the line shape of L_{12} . There have been many reports that metallic impurities can significantly affect the thermoelectric properties [16,20,21]. Figure S6 compares the line shapes of L_{12} for the 100% (6,5) SWCNTs and mixed samples with metallic SWCNTs (9:1 and 1:1). These L_{12} line shapes are derived from the data of S and σ in Ref. [11]. According to the results, the slight presence of metallic SWCNTs significantly influences the peak structure of L_{12} . Only a 10% inclusion of metallic SWCNTs in the thin film decreases the value of L_{12} over the entire range, while a 50% inclusion completely eliminates the peak structure. In

the present study, the purity of the (6,5) SWCNTs is greater than 99%, whereas the purities of the other semiconducting SWCNTs are not (see Fig. S7 of the SM). Therefore, we may assume that the presence of metallic SWCNTs or other chiral SWCNT impurities will influence the decrease in the L_{12} peak structure results of semiconducting SWCNT thin films.

From the above discussion, we find that L_{12} is an important parameter for discussing the dimensionality of thermoelectric properties, but it should be further noted that L_{12} is also an important parameter for improving the thermoelectric performance. The power factor ($= S^2\sigma$) can be expressed using L_{12} as $P = (L_{12})^2/T^2\sigma$. According to this equation, to improve the value of P , it is necessary to prepare materials with a large L_{12} and a small σ . A small σ also leads to a small thermal conductivity; thus, finding materials with a large L_{12} at a small σ is a good strategy for improving the thermoelectric performance. In fact, recently the enhancement of thermoelectric generation using the anomalous Nernst effect was reported in iron-based materials [22], and the enhancement was found to be due to the large increase in L_{12} . Therefore, the understanding of L_{12} in materials will help us to understand the background of thermoelectric phenomena and to improve the thermoelectric performance.

III. CONCLUSIONS

In summary, the present study discusses how the dimensionalities of low-dimensional semiconductor electronic structures influence the thermoelectric properties. In the line shape of conventional thermoelectric parameters, such as S and P , it is very difficult to find traces of the dimensionality of the electronic structure. However, the thermoelectrical conductivity, L_{12} , strongly depends on the line shape of the DOS, and we can evaluate the dimensionality of the sample from the L_{12} line shape. We find that L_{12} of the (6,5) SWCNTs exhibits a unique character that reflects the 1D electronic structure: the peak structure of L_{12} reflects the presence of a sharp DOS due to a vHs. Our results indicate the importance of L_{12} for understanding the relationships between the semiconducting electronic structure and thermoelectric properties. In addition,

our results imply that the 1D properties of nanomaterials can also be observed at a macroscopic scale, such as in films. This fact can be beneficial for promoting the potential thermoelectric application of 1D materials and encouraging further research.

IV. METHODS

A. SWCNT film preparation and device fabrication for evaluation of thermoelectric properties

High-purity semiconducting (6,5), (9,4), and (10,3) SWCNTs were prepared through gel chromatography from the original SWCNTs synthesized by the CoMoCAT[®] method (SG65, Sigma-Aldrich) for (6,5) and by HiPco (HiPco Raw SWNTs HR32-166, NanoIntegris) for (9,4) and (10,3). The details of these separation procedures can be found in Ref. [13]. Semiconducting SWCNTs (Semi) and metallic SWCNTs with a diameter of 1.4 nm, which was used in the purity dependence experiments (Fig. S6), were prepared using density gradient ultracentrifugation from the original SWCNTs synthesized by the arc-discharge method (Arc SO, Meijyo Nano Carbon Co.). In the purity dependence experiments, we prepared samples by mixing the (6,5) and metallic SWCNTs. The optical absorbance spectra for all samples can be found in Fig. S7. The films were prepared using conventional transfer techniques using a polycarbonate membrane filter (Whatman Nuclepore Track-Etched membrane 25 mm 0.2 μm) to form a thin film.

The fabrication processes of the devices for thermoelectric measurements were the same as those in Ref. [11] in the main text. We used a combined method of electrolyte gating and thermoelectric measurements, which we reported previously. We used an ionic liquid (TMPA-TFSI, Kanto Chemical Co.) for the electrolyte. All the measurements were conducted in vacuum ($\sim 10^{-3}$ Pa) using a vacuum and low-temperature probe station (Grail 10, Nagase Techno Co.). Although S and σ values of (6,5) have already been evaluated in Ref. [11], we prepared another (6,5) sample with the same high purity ($>99\%$) for this study to evaluate its L_{12} , S , and σ . In addition, we clarified the thermoelectric properties of (9,4), (10,3), and Semi SWCNTs and evaluated the L_{12} values.

B. Theoretical calculations using Kubo-Luttinger theory

Based on the Kubo-Luttinger formula [23,24], L_{11} and L_{12} of a single-electron system can be expressed as the Sommerfeld-Bethe relations [8,16,25–27]:

$$L_{11} = \int_{-\infty}^{\infty} dE \left(-\frac{\partial f(E - \mu)}{\partial E} \right) \alpha(E) \quad (3)$$

and

$$L_{12} = -\frac{1}{e} \int_{-\infty}^{\infty} dE \left(-\frac{\partial f(E - \mu)}{\partial E} \right) (E - \mu) \alpha(E), \quad (4)$$

where e is the elementary charge, $f(E - \mu)$ is the Fermi-Dirac distribution function, and $\alpha(E)$ is the spectral conductivity. Using L_{11} and L_{12} , S and P are expressed as

$$S = \frac{1}{T} \frac{L_{12}}{L_{11}} \quad (5)$$

and

$$P = L_{11} S^2 = \frac{1}{T^2} \frac{L_{12}^2}{L_{11}}. \quad (6)$$

An effective Hamiltonian of SWCNTs is known to be expressed as a 1D free Dirac Hamiltonian, which is given by

$$H_0(k) = \begin{pmatrix} \Delta & \hbar v k \\ \hbar v k & -\Delta \end{pmatrix}, \quad (7)$$

where Δ is half of the band gap, v is the velocity of a Dirac electron in the high-energy region of $|E| \gg \Delta$, k is the wave number of a Dirac electron, and $\hbar = h/2\pi$ is the Dirac constant [8]. In the self-consistent Born approximation for short-range random potential, $\alpha(E)$ and $\rho(E)$ can be analytically calculated by

$$\alpha(E) = \frac{1}{A} \frac{e^2}{h} \frac{1}{\text{Im}(\kappa_1 \kappa_2)} \text{Re} \left\{ \frac{2\kappa_1 \kappa_2 + \kappa_1^* \kappa_2 + \kappa_1 \kappa_2^*}{\sqrt{\kappa_1 \kappa_2}} \right\} \quad (8)$$

with $\text{Im}\sqrt{\kappa_1 \kappa_2} > 0$, and

$$\rho(E) = \frac{a}{2\pi \hbar v} \text{Re} \left\{ \frac{\kappa_1 + \kappa_2}{\sqrt{\kappa_1 \kappa_2}} \right\}, \quad (9)$$

where A is the cross-sectional area of the system, a is the unit-cell length,

$$\kappa_1 \equiv \frac{E - \Delta - \sum_{11}^{\text{R}}(E)}{\hbar v}, \quad (10)$$

and

$$\kappa_2 \equiv \frac{E + \Delta - \sum_{22}^{\text{R}}(E)}{\hbar v}. \quad (11)$$

$\sum_{11}^{\text{R}}(E)$ and $\sum_{22}^{\text{R}}(E)$ are the diagonal elements of the retarded self-energy matrix. This calculation procedure was conducted in Figs. 3(a), S3, and S4. In Fig. S4, the red, blue, green, and pink curves correspond to (6,5) SWCNTs, (9,4) SWCNTs, (10,3) SWCNTs, and (11,10) SWCNTs, respectively, with relaxation times of 100 fs.

ACKNOWLEDGMENTS

We thank Hidetoshi Fukuyama for valuable discussions, and Kanna Ikoma, Hitomi Okubo, and Junko Eda for their support with the sample preparations. K.Y. acknowledges support by JSPS KAKENHI through Grants No. JP17H06124, No. JP17H01069, No. JP18H01816, and No. JP20H02573. T.Y. acknowledges support by JSPS KAKENHI through Grant No. JP18H01816. Y.I. acknowledges support by JSPS KAKENHI through Grant No. JP19J21142. M.M. acknowledges support by JSPS KAKENHI through Grant No. JP 20K15117. T.T. acknowledges support by JSPS KAKENHI (Grants No. JP20H05664, No. JP20H05867, No. JP19K22127, and No. JP17H01069). J.P. acknowledges support by JSPS KAKENHI Grants No. JP19K15383 and No. JP20H05189. K.Y., T.T., and T.Y. acknowledge support by JST CREST through Grant No. JPMJCR17I5, Japan.

- [1] J.-H. Bahk, H. Fang, K. Yazawa, and A. Shakouri, *J. Mater. Chem. C* **3**, 10362 (2015).
- [2] M. Dresselhaus, G. Chen, M. Tang, R. Yang, H. Lee, D. Wang, Z. Ren, J.-P. Fleurial, and P. Gogna, *Adv. Mater.* **19**, 1043 (2007).
- [3] L. D. Hicks and M. S. Dresselhaus, *Phys. Rev. B* **47**, 16631 (1993).
- [4] G. Mahan and J. Sofo, *Proc. Natl. Acad. Sci. (USA)* **93**, 7436 (1996).
- [5] D. Li, Y. Wu, R. Fan, P. Yang, and A. Majumdar, *Appl. Phys. Lett.* **83**, 3186 (2003).
- [6] B. Poudel, Q. Hao, Y. Ma, Y. Lan, A. Minnich, B. Yu, X. Yan, D. Wang, A. Muto, D. Vashaee, X. Chen, J. Liu, M. S. Dresselhaus, G. Chen, and Z. Ren, *Science* **320**, 634 (2008).
- [7] N. F. Mott and E. A. Davis, *Electronic Processes in Non-Crystalline Materials*, 2nd ed. (Oxford University Press, Oxford, 1979).
- [8] T. Yamamoto and H. Fukuyama, *J. Phys. Soc. Jpn.* **87**, 114710 (2018).
- [9] See Supplemental Material at <http://link.aps.org/supplemental/10.1103/PhysRevMaterials.5.025404> for the detailed calculation method.
- [10] J. L. Blackburn, A. J. Ferguson, C. Cho, and J. C. Grunlan, *Adv. Mater.* **30**, 1704386 (2018).
- [11] Y. Ichinose, A. Yoshida, K. Horiuchi, K. Fukuhara, N. Komatsu, W. Gao, Y. Yomogida, M. Matsubara, T. Yamamoto, J. Kono, and K. Yanagi, *Nano Lett.* **19**, 7370 (2019).
- [12] K. Yanagi, S. Kanda, Y. Oshima, Y. Kitamura, H. Kawai, T. Yamamoto, T. Takenobu, Y. Nakai, and Y. Maniwa, *Nano Lett.* **14**, 6437 (2014).
- [13] Y. Ichinose, J. Eda, Y. Yomogida, Z. Liu, and K. Yanagi, *J. Phys. Chem. C* **121**, 13391 (2017).
- [14] M. S. Arnold, A. A. Green, J. F. Hulvat, S. I. Stupp, and M. C. Hersam, *Nat. Nanotechnol.* **1**, 60 (2006).
- [15] J. Pu, K. Kanahashi, N. T. Cuong, C.-H. Chen, L.-J. Li, S. Okada, H. Ohta, and T. Takenobu, *Phys. Rev. B* **94**, 014312 (2016).
- [16] T. Yamamoto and H. Fukuyama, *J. Phys. Soc. Jpn.* **87**, 024707 (2018).
- [17] M. Ogata and H. Fukuyama, *J. Phys. Soc. Jpn.* **88**, 074703 (2019).
- [18] K. Kanahashi, M. Ishihara, M. Hasegawa, H. Ohta, and T. Takenobu, *npj 2D Mater. Appl.* **3**, 44 (2019).
- [19] H. Dumlich, M. Gegg, F. Hennrich, and S. Reich, *Phys. Status Solidi B* **248**, 2589 (2011).
- [20] A. Avery, B. Zhou, J. Lee, E. Lee, E. Miller, R. Ihly, D. Wesenberg, K. Mistry, S. Guillot, B. L. Zink, Y. Kim, J. L. Blackburn, and A. Ferguson, *Nat. Energy* **1**, 16033 (2016).
- [21] D. Hayashi, T. Ueda, Y. Nakai, H. Kyakuno, Y. Miyata, T. Yamamoto, T. Saito, K. Hata, and Y. Maniwa, *Appl. Phys. Express* **9**, 025102 (2016).
- [22] A. Sakai, S. Minami, T. Koretsune, T. Chen, T. Higo, Y. Wang, T. Nomoto, M. Hirayama, S. Miwa, D. Nishio-Hamane, F. Ishii, R. Arita, and S. Nakatsuji, *Nature (London)* **581**, 53 (2020).
- [23] R. Kubo, *J. Phys. Soc. Jpn.* **12**, 570 (1957).
- [24] J. M. Luttinger, *Phys. Rev.* **135**, A1505 (1964).
- [25] M. Jonson and G. D. Mahan, *Phys. Rev. B* **21**, 4223 (1980).
- [26] H. Kontani, *Phys. Rev. B* **67**, 014408 (2003).
- [27] M. Ogata and H. Fukuyama, *J. Phys. Soc. Jpn.* **86**, 094703 (2017).